

Deep Learning Based Packet Detection and Carrier Frequency Offset Estimation in IEEE 802.11ah

Vukan Ninkovic, Dejan Vukobratovic
*Faculty of Technical Sciences
 University of Novi Sad
 Novi Sad, Serbia
 email: {ninkovic,dejanv}@uns.ac.rs*

Aleksandar Valka, Dejan Dumic
*Methods2Business
 Novi Sad, Serbia
 email: {aleksandar,dejan}@methods2business.com*

Abstract—Data-based machine learning methods are currently disrupting communication engineering physical layer research. Promising results have been presented in the recent literature, in particular in the domain of deep learning-based channel estimation. In this paper, we investigate deep neural network (DNN)-based solutions for packet detection and carrier frequency offset (CFO) estimation. We focus on preamble-based OFDM systems such as IEEE 802.11, and apply the investigated DNN-based methods in emerging IEEE 802.11ah standard. Our investigation, performed within a detailed standard-based simulated environment, demonstrates competitive performance of DNN-based methods as compared to the conventional ones. In particular, convolutional neural network and recurrent neural network architectures applied in packet detection and CFO estimation, respectively, demonstrated robustness and accuracy that matched and even surpassed the conventional methods.

Index Terms—Deep Learning, Carrier Frequency Offset Estimation, Packet Detection, IEEE 802.11ah

I. INTRODUCTION

Wireless communication systems based on the orthogonal frequency division multiplexing (OFDM) dominate current wireless research and development, underlying the latest mobile cellular and Wi-Fi standards. Conventional model-based signal processing methods at OFDM receivers are well understood and are currently used as a basis for receiver design [1]–[6]. Recently, these methods are challenged by the data-based approaches relying on deep neural networks (DNN) [7]–[9]. DNN-based methods have been evaluated across various domains of physical layer (PHY) processing, ranging across signal detection [10], channel estimation [11] and error correction coding [12], demonstrating promising performance as compared to the conventional methods.

Among receiver-side PHY procedures, DNN-based channel estimation received most attention, targeting modern scenarios such as massive MIMO and mmWave systems [13]. Higher-level positioning services that use channel state information as a fingerprint have also been well explored recently [14]. However, in most of the DNN-based PHY studies, signal detection at the receiver that includes procedures that precede channel estimation, such as carrier frequency offset (CFO) or signal timing related estimations, are assumed perfect. Indeed, only a few recent studies use DNN methods to challenge conventional algorithms in the domain of CFO and

timing estimation [10], [15]. In addition, studies on DNN-based methods focusing specifically on preamble-based listen-before-talk (LBT) OFDM systems are also missing, with only a few exceptions in the domain of channel estimation [16].

In this paper, we fill this gap by focusing on DNN-based OFDM signal detection in IEEE 802.11 systems, targeting packet detection and CFO estimation methods. In order to provide detailed standard-specific investigation, we consider emerging IEEE 802.11ah standard for low-power Internet of Things (IoT) applications [17]. We investigate different DNN-based solutions for packet detection and CFO estimation, and compare them to the conventional methods. For the performance evaluation, a detailed standard-based IEEE 802.11ah simulated environment is used, where competitive performance of DNN-based methods, as compared to the conventional ones, is demonstrated. In particular, for CFO estimation within the IEEE 802.11ah receiver, long short-term memory (LSTM)-based recurrent neural network (RNN) are able to match the performance of conventional methods, and even surpass them in low-to-medium signal-to-noise ratio (SNR). Similarly, for packet detection, one-dimensional convolutional neural (CNN) networks demonstrates accuracy that surpasses the conventional methods.

The paper is organized as follows. In Sec. II, we present system model and review IEEE 802.11ah frame structure. Next two sections present details on DNN-based CFO estimation (Sec. III) and packet detection (Sec. IV), where each section starts by reviewing conventional methods. Performance results are presented in Sec. V, followed by concluding remarks.

II. BACKGROUND AND SYSTEM MODEL

OFDM Communication System Model: We consider an OFDM system with N subcarriers separated by Δf in the frequency domain. At the transmitter, the binary information sequence is mapped onto the complex modulation symbols, which are allocated to different subcarriers and converted into the time-domain signal via the Inverse Discrete Fourier Transform (IDFT) [1]. The resulting discrete-time complex baseband signal x_n can be expressed as:

$$x_n = \frac{1}{N} \sum_{k=0}^{N-1} X_k e^{\frac{j(2\pi kn)}{N}}, \quad n = 0, 1, \dots, N-1, \quad (1)$$

where X_k is the complex signal in the frequency domain.

Cyclic prefix (CP) of length greater than the channel delay spread is inserted and signal is oversampled and filtered before the oversampled signal \mathbf{x}_{os} is passed through the indoor multi-path channel. Focusing on the discrete-time complex-baseband model, the channel is represented via its discrete-time impulse response \mathbf{h} . After adding complex Additive White Gaussian Noise (AWGN) \mathbf{w} samples, the signal obtained at the receiver is:

$$\mathbf{y}_{os} = \mathbf{x}_{os} \circledast \mathbf{h} + \mathbf{w}, \quad (2)$$

where \circledast represents the circular convolution.

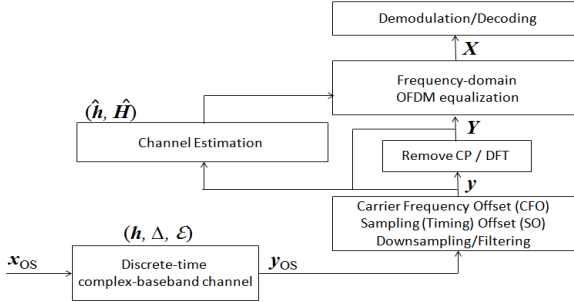


Fig. 1. OFDM Wireless Receiver.

At the receiver side, which is the focus of this paper, after the signal passes through the reverse pulse-shape filtering and downsampling, CFO and timing synchronization are applied (Fig. 1). Following cyclic prefix removal and DFT, the received frequency-domain signal equals:

$$Y_k = \sum_{n=0}^{N-1} y_n \cdot e^{-j(2\pi k n)}, \quad k = 0, 1, \dots, N-1 \quad (3)$$

Next, signal correction aided by channel estimation (usually based on inserted pilot symbols) is executed and the data is passed to demodulation and channel decoding. Lastly, the binary information data is obtained back.

Note that, besides the channel impairment and the noise, the received signal (\mathbf{y}_{os}) is affected by the time sampling offset ϵ and CFO Δ which needs to be estimated and corrected. A CFO of $\Delta = f_{off}/\Delta f$ causes a phase rotation of $2\pi t f_{off}$. If uncorrected, this causes both a rotation of the constellation and a spread of the constellation points. A timing error ϵ will have a little effect as long as all the taken samples are within the length of the cyclically-extended OFDM symbol [3].

IEEE 802.11ah Frame Structure: In this paper, we focus on a listen-before-talk (LBT)-based IEEE 802.11 OFDM technologies. In LBT systems, the sequence of data symbols is preceded by a preamble of known data needed for initial synchronization and/or channel estimation (Fig. 2). The initial synchronization includes the frame detection, i.e., estimation of the initial time sample of the incoming frame, and CFO estimation. Preamble structure is usually based on repeated patterns of symbols with good correlation properties [4].

For the purpose of detailed implementation and evaluation, but without loss of generality, we restrict our attention on the

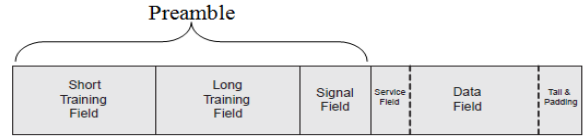


Fig. 2. IEEE 802.11 frame structure.

IEEE 802.11ah (*Wi-Fi HaLow*) standard [17]. Therein, for 1 MHz packet structure, a fixed-length packet preamble contains 14 OFDM symbols, where every OFDM symbol has $N = 32$ subcarriers at spacing $\Delta f = 31.25$ kHz. Normal cyclic prefix of $8\mu s$ duration is applied, resulting in $40\mu s$ OFDM symbol. The preamble follows 802.11 structure adapted to specific 802.11ah requirements:

Short Training Field (STF) - STF lasts $160\mu s$ and consists of 4 OFDM symbols which, after IDFT, represent 10 repetitions of the same $16\mu s$ -long short training symbol (STS). STS is of good correlation properties and low peak-to-average power is preserved even after clipping or compression by an overloaded analog front end. STF is suitable for coarse timing synchronization and coarse CFO estimation.

Long Training Field 1 (LTF1) - LTF1 also contains 4 OFDM symbols of $160\mu s$ duration. Two repetitions of the same long training symbol enable fine timing synchronization, CFO estimation and channel estimation.

Signal Field (SIG) contains packet information to configure the receiver: rate (modulation and coding), length, etc., while **Long Training Field 2 (LTF2)** is used for MIMO channel estimation, and is not relevant in our case as we focus on single-antenna (SISO) transmission.

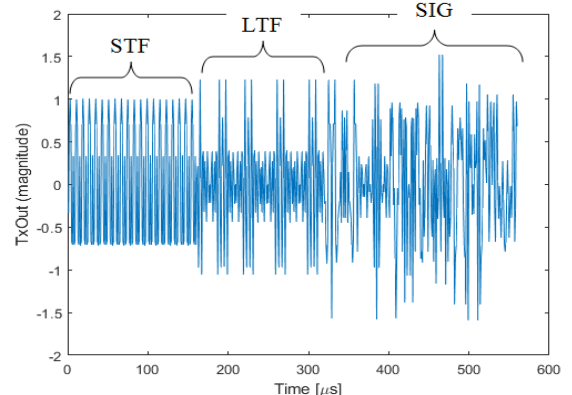


Fig. 3. 802.11ah NDP packet transmit waveform.

In this work, we focus on initial synchronization, which depends only on the packet preamble. In order to reduce the simulation burden, we use 802.11ah Null Data Packets (NDP) [4], that contain only the preamble without data field (Fig. 3).

III. DNN-BASED CFO ESTIMATION

We first consider the problem of CFO estimation from the IEEE 802.11ah preamble, assuming perfect packet detection.

Before considering the details of suitable DNN architectures, we briefly review conventional CFO methods.

Conventional CFO Estimation Methods: A common approach to CFO estimation, proposed in [5], uses the fact that the samples of two consecutively received identical symbols differ by the phase shift proportional to the CFO f_{off} :

$$y_{n+L} = y_n e^{j2\pi f_{off} T_s}, \quad (4)$$

where L represents the length of a training symbol and T_s is the sample period. Maximum likelihood CFO estimate uses complex correlation Λ_τ between the repeated symbols:

$$\Lambda_\tau = \sum_{n=\tau}^{\tau+L-1} y_n^* y_{n+L} \quad (5)$$

Further improvements of this algorithm use the phase of Λ_τ , denoted as $\hat{\phi} = \angle(\Lambda_\tau)$, to estimate CFO [3], [6]:

$$\hat{f}_{off} = \frac{f_s \hat{\phi}}{2\pi N}, \quad (6)$$

where $f_s = \frac{N}{T_s}$ is the sample frequency. Since $\hat{\phi}$ that can be estimated without phase ambiguity is restricted to $\hat{\phi}_{max} = \pm\pi$, the maximum estimated CFO equals $\frac{\Delta f}{2}$ [6].

In IEEE 802.11ah, the CFO estimation is separated into two steps. The coarse CFO, denoted as $\hat{f}_{off}^{(1)}$, is carried out using auto-correlation of two adjacent STS within STF, taken at the estimated packet start sample time τ_S [18]:

$$\Lambda_{\tau_S}^{(1)} = \sum_{n=\tau_S}^{\tau_S+L-1} y_n^* y_{n+l_S} = e^{\frac{j2\pi \hat{f}_{off}^{(1)} l_S}{f_s}} \sum_{n=\tau_S}^{\tau_S+L-1} |y_n|^2 \quad (7)$$

where l_S is the STS sample-length and L is equal to or is a multiple of l_S . Using (6) and (7), and $\hat{\phi}^{(1)} = \angle(\Lambda_{\tau_S}^{(1)})$, we get:

$$\hat{f}_{off}^{(1)} = \frac{f_s}{2\pi l_S} \hat{\phi}^{(1)}. \quad (8)$$

After correcting $\hat{f}_{off}^{(1)}$ over the signal \mathbf{y} (obtained after filtering and downsampling \mathbf{y}_{os}), the coarse CFO-compensated signal $\hat{\mathbf{y}}$ is obtained. Using LTF field of $\hat{\mathbf{y}}$, the fine CFO estimation $\hat{f}_{off}^{(2)}$ is obtained [18]:

$$\Lambda_{\tau_L}^{(2)} = \sum_{n=\tau_L}^{\tau_L+L_L-1} \hat{y}_n^* \hat{y}_{n+l_L} = e^{\frac{j2\pi \hat{f}_{off}^{(2)} l_L}{f_s}} \sum_{n=\tau_L}^{\tau_L+L_L-1} |\hat{y}_n|^2, \quad (9)$$

where $\tau_L = \tau_S + L_S$ is the initial LTF sample, L_S and L_L are sample-lengths of STF and LTF field, and l_L is a sample length of a long training symbol. Using $\hat{\phi}^{(2)} = \angle(\Lambda_{\tau_L}^{(2)})$ the fine CFO is estimated as:

$$\hat{f}_{off}^{(2)} = \frac{f_s}{2\pi l_L} \hat{\phi}^{(2)} \quad (10)$$

Finally, the CFO of the received signal is estimated as the sum of the coarse and fine CFOs: $\hat{f}_{off} = \hat{f}_{off}^{(1)} + \hat{f}_{off}^{(2)}$.

DNN Architectures for CFO Estimation: Next, we detail the DNN architectures we consider for CFO estimation.

1) ReLU DNN: Fully connected (FC) feedforward neural network, which consists of input, output and hidden layers, represents a simple and well-understood DNN model. The relation between the input \mathbf{x} and the output \mathbf{y} is a layer-wise composition of computational units in the form of:

$$\mathbf{y} = f(\mathbf{x}, \Theta) = f_o(g_{M-1}(\dots(g_1(f_1(\mathbf{x}))))), \quad (11)$$

where Θ denotes the set of network parameters (weights \mathbf{W}_i and biases \mathbf{b}_i), $f_i(\mathbf{x}) = \mathbf{W}_i \mathbf{x} + \mathbf{b}_i$ and $g_i(\cdot)$ are the linear pre-activation and activation function of the i_{th} hidden layer, respectively, $f_o(\cdot)$ represents the linear function of the output layer, and M is the number of layers. Among the non-linear activation functions, we focus on rectified linear units (ReLU), as ReLU DNNs are known universal piece-wise linear function approximators for a large class of functions [19].

2) Recurrent Neural Networks (RNN): RNNs represent sequence-based models able to establish temporal correlations between the previous and the current circumstances. A simple example of a single-layer RNN is given in Fig. 4, where the output of the previous time step $t-1$ becomes a part of the input of the current time step t , thus capturing past information. Computation result performed by one RNN cell can be expressed as following function [20]:

$$\mathbf{h}_t = \tanh(\mathbf{W}_{ih} \mathbf{x}_t + \mathbf{b}_{ih} + \mathbf{W}_{hh} \mathbf{h}_{t-1} + \mathbf{b}_{hh}), \quad (12)$$

where \tanh represents the hyperbolic tangent function, \mathbf{h}_t and \mathbf{h}_{t-1} are the hidden states at time steps t and $t-1$, respectively, \mathbf{W}_{ih} , \mathbf{W}_{hh} and \mathbf{b}_{ih} , \mathbf{b}_{hh} are weights and biases which need to be learned, and input at time t is denoted as \mathbf{x}_t .

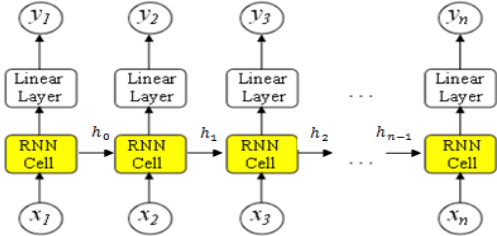


Fig. 4. The structure of Recurrent Neural Network.

Basic RNN cells fail to learn long-range dependencies due to the vanishing or exploding gradients. To solve this, Long Short-Time Memory (LSTM) cells are put forward that contain special units called *memory blocks* in recurrent hidden layer, which enhance its capability to model long-term dependencies [21]. This block is a recurrently connected subnet that contains functional modules called memory cells and gates. The former remember the network temporal state while the latter control the information flow from the previous cell state.

Besides standard LSTM cells, we also consider Gated Recurrent Unit (GRU) [22]. The main ideas from LSTMs are preserved, but GRU introduces only two gates, update gate and reset gate, to control the information flow. GRUs perform similarly to LSTM, but with reduced execution time [23].

Data Set and Training Procedure: In this paper, we test the ability of selected DNN architectures to estimate the CFO from the phase of received STF samples:

$$\hat{f}_{off} = f(\angle(\mathbf{y}_{STF})). \quad (13)$$

We use the following data set: $(\angle(\mathbf{y}_{STF}), f_{off})$, where f_{off} represents a real CFO introduced during the transmission. A DNN architecture tries to learn the mapping between the received $\angle(\mathbf{y}_{STF})$ and f_{off} , where, in our case, $f_{off} \in [-\frac{\Delta f}{2}, \frac{\Delta f}{2}] = [-15.625 \text{ kHz}, 15.625 \text{ kHz}]$. Note that we test our DNN-based CFO estimation only on STF field, unlike conventional methods that use both STF and LTF fields.

After downsampling and filtering, \mathbf{y}_{STF} consists of 160 samples (10 repetitions of 16-sample STS). We collected 50,000 received NDP packets and extracted STF phase vectors, and the corresponding true CFO values generated uniformly at random. From the data set, 70% records are used for training, 15% for validation and 15% for testing purposes. To examine estimator robustness, NDP packets are received with different SNRs, between 0 dB and 25 dB. Depending on the simulated channel model, two data sets are created: i) AWGN channel, and ii) indoor multipath fading channel - model B [24].

To train DNN models, we minimized the mean-squared error (MSE) loss: $L_{MSE}(f_{off}, \hat{f}_{off}) = \sum_i (f_{off,i} - \hat{f}_{off,i})^2$, providing better performance than mean-absolute error (MAE) and Huber loss. The training set is divided into mini-batches of size 100, and 500 epochs are sufficient for the loss function convergence. Network parameters are optimized using stochastic gradient descent (SGD) algorithm with ADAM optimizer at the learning rate $\alpha = 0.001$, $\beta_1 = 0.9$ and $\beta_2 = 0.999$ [25].

The ReLU DNN includes five layers: an input layer of 160 neurons, three hidden layers with 32, 64 and 16 neurons, respectively, and an output single-neuron layer. The RNN consists of one LSTM or GRU layer with 30 units followed by one ReLU FC layer with 5 neurons and an output layer with a single neuron. Unlike ReLU DNN, where the input is the whole sequence $\angle(\mathbf{y}_{STF})$, at RNN, this sequence is separated into STSs (16 samples), and one STS is input into one LSTM/GRU unit.

IV. DNN-BASED PACKET DETECTION

In the previous section, perfect packet detection is assumed. Next, we design DNN-based algorithms for packet detection.

Conventional Packet Detection Methods: Conventional packet detection also exploits repetitive preamble structure and correlation between two subsequent training symbols. In [3] and [6], authors noted that the product of each of these sample pairs at the start of the frame will have approximately the same phase, so the magnitude of the sum will be large. They introduced a window of $2L$ samples sliding in time searching for the packet start sample τ_S using timing metric:

$$M(\tau) = \frac{|\Lambda_\tau|^2}{P_\tau^2}, \quad (14)$$

where $P_\tau = \sum_{i=0}^{L-1} |y_{\tau+i}|^2$.

The first method simply finds the time sample that maximizes the timing metric $M(\tau)$, while the second one, except finding maximum, observes the points to the left and right in the time domain which exceed 90% of the maximum value, and average these two 90% times to get the appropriate timing estimation. In order to avoid false detection, a threshold should be set that triggers the above algorithm.

In IEEE 802.11, conventional methods are adapted to specific requirements. For example, coarse packet detection may follow [3], setting $L = 80$ samples (one half of STF duration):

$$\begin{aligned} \hat{\tau}_S &= \arg \max_{\tau} \frac{|\Lambda_\tau|^2}{(P_\tau)^2} \\ &= \arg \max_{\tau} \left(\frac{|\sum_{n=\tau}^{\tau+L_S-l_S} y_n^* y_{n+l_S}|^2}{(\sum_{n=\tau}^{\tau+L_S-l_S} |y_n|^2)^2} \right). \end{aligned} \quad (15)$$

DNN Architectures for Packet Detection: For packet detection, besides the baseline ReLU DNN, we consider one-dimensional convolutional neural network (1D-CNN) known to provide excellent results in processing time series data.

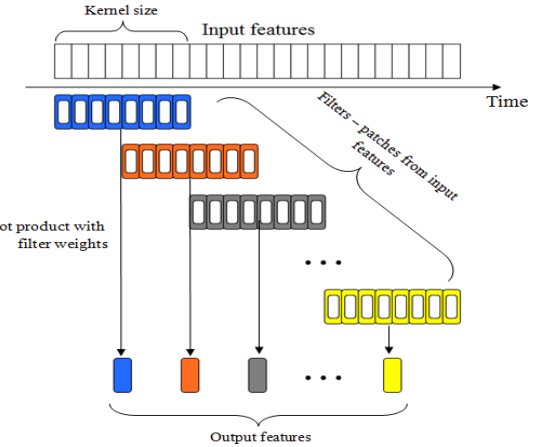


Fig. 5. Structure of 1D convolution layer.

1) Convolutional Neural Network (1D): CNNs are known to achieve superb performances on computer vision and image classification problems by extracting features from local input patches, that form more complex patterns at higher layers [26]. Similar approach can be applied for 1D-sequences of data, with 1D-CNN being effective in deriving features from shorter segments of the data set. For packet detection problem, it is important to notice that 1D convolution layers are translation invariant, because the same input transformation is performed on every patch, and a pattern learned at a certain position in the signal can be latter recognized at a different position.

Two types of layers are applied in compact 1D-CNNs: i) 1D-CNN layer, where 1D convolution occurs, and ii) FC layer. Each hidden CNN layer performs a sequence of convolutions, whose sum is passed through the activation function [27]. At the end, CNN layers process the raw 1D data and extract features used by FC layers for prediction tasks (Fig. 5). Compared

to 2D-CNNs, 1D-CNN can use larger filter and convolution window sizes with lower computational complexity.

Data Set and Training Procedure: In packet detection, DNN needs to learn mapping between the input signal and the output value representing the packet start sample while distinguishing from the noise. We assume that DNN-based packet detection operates over the consecutive fixed-length blocks of the received signal amplitude:

$$\hat{\tau}_S = f(|\mathbf{y}|), \quad (16)$$

after the received signal is downsampled and filtered.

The received signal is segmented into the input blocks \mathbf{y} of 1600 samples, while the packet start instant τ_S is set uniformly at random among input samples. The data set consists of $(|\mathbf{y}|, \tau_S)$ pairs. Two data sets are created, under the same channel models as in Sec. III.C, containing 30,000 samples (70% for training, 15% for validation and 15% for testing). MSE loss function is used as it again provides the best performances. Mini-batch size is set to 50, and the training lasts 500 epochs, where SGD with ADAM optimizer is implemented with same hyperparameters as in Sec. III.C.

TABLE I
1D-CNN NETWORK PARAMETERS FOR PACKET DETECTION.

Layer	Size (number of filters/neurons)
Conv1D + ReLU	30
Conv1D + ReLU	10 (filter size is 5 samples)
FC + ReLU	5
Output (Linear)	1

For ReLU DNN, after the input layer of 1600 neurons that takes the whole block $|\mathbf{y}|$, 3 hidden layers and 1 output layer of the same structure as in Sec. III.C are applied. Note that the size of the input layer is subject to optimization. Using larger input blocks increases the complexity of the first layer, but reduces the number of blocks to be processed per unit time (note that conventional algorithms use sample-by-sample processing of input blocks of size 80). Careful investigation of the above trade offs is left for future work.

As a reduced input size solution, 1D-CNN uses a convolution layer filter of length 80 samples with 40 samples stride (Fig. 5). The layer parameters are set as in Table I.

V. NUMERICAL RESULTS

In this section, we conduct performance evaluation of the proposed DNN-based methods for CFO estimation and packet detection, and compare them with conventional methods in terms of the mean absolute error (MAE) under different SNRs.

CFO estimation: Mean absolute error (MAE) of CFO estimation as a function of channel SNR is presented in Fig. 6 and Fig. 7 for both channel models (Sec. III.C), respectively. DNN-based methods use only STF samples, while conventional methods use both STF+LTF samples (i.e., both coarse and fine CFO). From the graphs, we note that certain DNN approaches are more robust to varying SNR values than the conventional algorithm, which however outperforms all DNN architectures

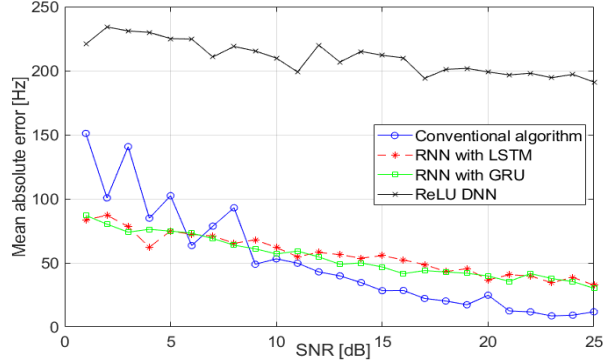


Fig. 6. MAE vs SNR for different algorithms under AWGN channel.

at the higher SNRs (above 8 dB). We also note that the more challenging indoor fading channel (model B) increases the MAE of all methods by approximately 15 Hz.

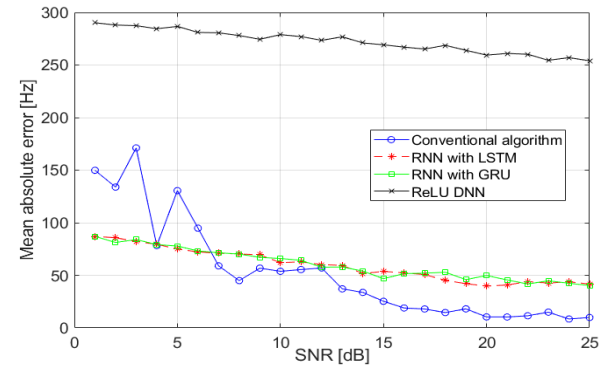


Fig. 7. MAE of different algorithms by SNR under indoor channel model.

We identify existence of outliers as the main reason why RNN is not able to follow the MAE performance of the conventional method at high SNRs. Indeed, taking a closer look at Fig. 8, the majority of test samples are predicted with high accuracy, except a few that deviate and badly affect MAE.

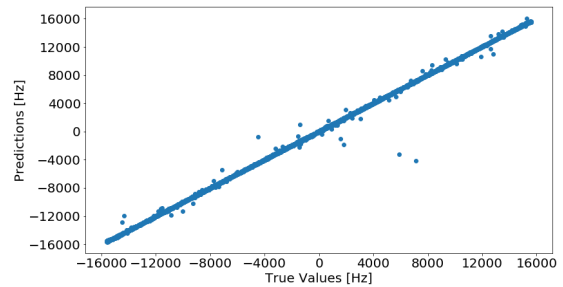


Fig. 8. True CFO values (x axis) vs predicted by RNN (y axis).

For the efficient CFO estimator, besides MAE, we need to consider the computational complexity. For DNN-based methods, it depends on the network trainable parameters: 8,705 for ReLU DNN, and 5,801 and 4,391 for RNN with LSTM and

GRU, respectively. Among the DNN-based methods, ReLU DNN has both the worst performance and complexity. RNN with GRU and LSTM cells have approximately the same MAE, where the latter has reduced complexity.

TABLE II
PACKET DETECTION MAE FOR AWGN/INDOOR CHANNELS.

Neural network	MAE (AWGN)	MAE (Indoor)
Conventional algorithm	0.82	1.7
Conv1D	0.74	2.42
ReLU DNN	3.05	2.69

Packet detection: MAE performance of the considered DNN architectures is able to match the conventional method, as illustrated in Table II, with 1D-CNN solution outperforming conventional method on AWGN channel. More detailed comparison of ReLU DNN and 1D-CNN networks are presented in Fig. 9 and Fig. 10 for two data sets, clearly showing adverse effects of indoor multipath channel model and better resilience of 1D-CNN packet detection performance. Finally, the number of trainable parameters used as a complexity measure is 25,601 and 54,401 for 1D-CNN and ReLU DNN, respectively.

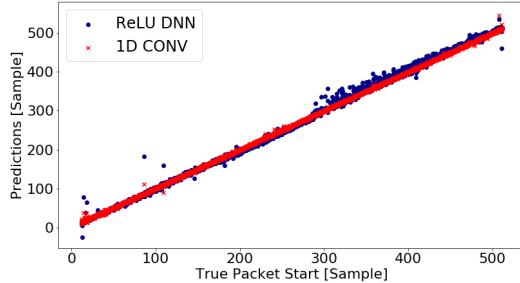


Fig. 9. Packet start sample estimation: true value (x-axis) vs predicted value (y axis) with 1D-CNN (red) and ReLU DNN (blue) for AWGN channel.

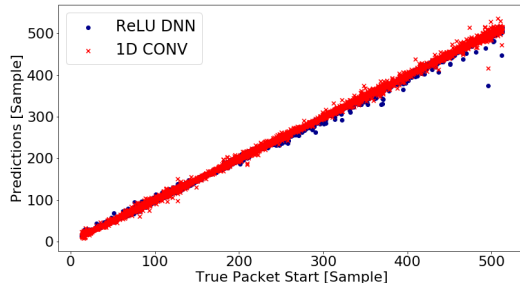


Fig. 10. Packet start sample estimation: true value (x-axis) vs predicted value (y axis) with 1D-CNN (red) and ReLU DNN (blue) for indoor channel.

VI. CONCLUSIONS

In this paper, we demonstrated robustness and efficiency of DNN-based packet detection and CFO estimation for IEEE 802.11ah signal detection. Our future work will fine-tune DNN parameters for optimized performance vs complexity and demonstrate results in real-world hardware implementation.

REFERENCES

- [1] J.-J. van de Beek, O. Edfors, M. Sandell, S.K. Wilson, and P.O. Borjesson, "On Channel Estimation in OFDM Systems," Proc. of Vech. Techn. Conf., pp. 815–819, 1995.
- [2] Y. Li, L.J. Cimini, and N.R. Sollenberger, "Robust channel estimation for OFDM systems with rapid dispersive fading channels," IEEE Trans. on Commun., vol 45, pp. 902–915, 1998.
- [3] T. M. Schmidl and D. C. Cox, "Robust frequency and timing synchronization for OFDM," IEEE Trans. on Commun., pp. 1613–1621, 1997.
- [4] K. S. Kim, S. W. Kim, Y. S. Cho, and J. Y. Ahn, "Synchronization and cell-search technique using preamble for OFDM cellular systems," IEEE Trans. Veh. Teh. Technol., vol. 56, pp. 34693485, 2007.
- [5] P. H. Moose, "A technique for orthogonal frequency division multiplexing frequency offset correction," IEEE Trans. Comm., 42(10), 1994.
- [6] A. van Zelst, and T. C. W. Schenck, "Implementation of a MIMO OFDM-based wireless LAN system," IEEE Trans. on Signal Processing, vol. 52, pp. 483–494, 2004.
- [7] T. Wang, C.-K. Wen, H. Wang, F. Gao, T. Jiang and S. Jin, "Deep Learning for Wireless Physical Layer: Opportunities and Challenges," IEEE/CIC ICCC, pp. 92-111, Beijing, China, Nov. 2017.
- [8] Z. Qin, H. Ye, G.Y. Li, B.H.F. Juang, "Deep learning in physical layer communications," IEEE Wireless Comm., 26(2), pp.93-99, 2019.
- [9] T. O'Shea, J. Hoydis, "An introduction to deep learning for the physical layer," IEEE Trans. Cogn. Comm. and Netw., 3(4), pp.563–575, 2017.
- [10] T. O'Shea, K. Karra, T.C. Clancy, "Learning approximate neural estimators for wireless channel state information," IEEE MLSP 2017, Japan.
- [11] H. Ye, G.Y. Li, B.H. Juang, "Power of deep learning for channel estimation and signal detection in OFDM systems," IEEE Wireless Communications Letters, 7(1), pp.114-117, 2017.
- [12] E. Nachmani, E. Marciano, L. Ligosch, W.J. Gross, D. Burshtein, Y. Beery, "Deep learning methods for improved decoding of linear codes," IEEE Journ. Sel. Topics Sign. Proc., 12(1), pp.119-131, 2018.
- [13] H. He, C.K. Wen, S. Jin, G.Y. Li, "Deep learning-based channel estimation for beamspace mmWave massive MIMO systems," IEEE Wireless Communications Letters, 7(5), pp.852-855, 2018.
- [14] X. Wang, L. Gao, S. Mao, S. Pandey, "CSI-based fingerprinting for indoor localization: A deep learning approach," IEEE Transactions on Vehicular Technology, 66(1), pp.763-776, 2016.
- [15] A. Li, Y. Me, S. Xue, N. Yi, R. Tafazolli, "A carrier-frequency-offset resilient OFDMA receiver designed through machine deep learning," IEEE PIMRC 2018, pp. 1-6, Bologna, Italy, 2018.
- [16] S. Han, Y. Oh, C. Song, "A Deep Learning Based Channel Estimation Scheme for IEEE 802.11 p Systems," IEEE ICC, Shanghai, China, 2019.
- [17] IEEE 802.11 ah-2016 Part 11: Wireless LAN Medium Access Control (MAC) and Physical Layer (PHY) Specifications - Amendment 2: Sub 1 GHz License Exempt Operation, December2016.
- [18] E. Perahia and R. Stacey, Next Generation Wireless LANs: Throughput, Robustness, and Reliability in 802.11n, Cambridge Univ. Press, 2008.
- [19] G. F. Montufar, R. Pascanu, K. Cho, and Y. Bengio, "On the number of linear regions of deep neural networks," NIPS, pp. 29242932., 2014.
- [20] Q. Bai, J. Wang, Y. Zhang, and J. Song, "Deep Learning-Based Channel Estimation Algorithm Over Time Selective Fading Channels," IEEE Trans. Cogn. Comm. and Netw., vol. 6, pp. 125-134, March 2020.
- [21] S. Hochreiter and J. Schmidhuber, "Long Short-Term Memory," Neural Computation, vol. 9, pp. 17351780, 1997.
- [22] K. Cho, B. van Merriënboer, C. Gulcehre, F. Bougares, H. Schwenk, and Y. Bengio, "Learning phrase representations using RNN encoder-decoder for statistical machine translation," Proc. of the Empirical Methods in Natural Language Processing (EMNLP), 2014.
- [23] K. Greff, R. K. Srivastava, J. Koutn, B. R. Steunebrink and J. Schmidhuber, "LSTM: A Search Space Odyssey," IEEE Trans. on Neural Networks and Learning Systems, vol. 28, pp. 2222-2232, 2017
- [24] R. Porat, S.K. Yong, K. Doppler. " IEEE P802.11 Wireless LANs TGah- Channel Model ", Proposed Text doc.: IEEE 802.1111/0968r4. 2015.
- [25] D. P. Kingma, J. L. Ba, "Adam: A method for stochastic optimization", Proc. Int. Conference on Learning Representation, pp. 1-41, 2015.
- [26] Y. LeCun, L. Bottou, Y. Bengio and P. Haffner, "Gradient-based learning applied to document recognition," in Proc. of the IEEE, vol. 86, pp. 2278-2324, 1998.
- [27] S. Kiranyaz, T. Ince, O. Abdeljaber, O. Avci and M. Gabbouj, "1-D Convolutional Neural Networks for Signal Processing Applications," ICASSP 2019, Brighton, UK, pp. 8360-8364., 2019.